

V^{IV} Disproportionation Upon Sodium Extraction From Na₃V₂(PO₄)₂F₃ Observed by *Operando* X-ray Absorption Spectroscopy and Solid State NMR

Thibault Broux ^{a,b,e}, Tahya Bamine ^{a,e}, Laura Simonelli ^c, Lorenzo Stievano ^{d,e,f},
François Fauth ^c, Michel Ménétrier ^{a,e}, Dany Carlier ^{a,e}, Christian Masquelier ^{b,e,f} and
Laurence Croguennec ^{a,e,f,*}

*Corresponding author (L. Croguennec): Laurence.Croguennec@icmcb.cnrs.fr

^a CNRS, Univ. Bordeaux, Bordeaux INP, ICMCB UPR 9048, F-33600 Pessac, France.

^b Laboratoire de Réactivité et de Chimie des Solides, CNRS-UMR#7314,
Université de Picardie Jules Verne, F-80039 Amiens Cedex 1, France

^c CELLS - ALBA synchrotron, E-08290 Cerdanyola del Vallès, Barcelona, Spain

^d CNRS, Univ. Montpellier, Institut Charles Gerhardt Montpellier UMR 5253,
F-34095 Montpellier Cedex 5, France

^e RS2E, Réseau Français sur le Stockage Electrochimique de l'Energie,
FR CNRS 3459, F-80039 Amiens Cedex 1, France

^f ALISTORE-ERI European Research Institute, FR CNRS 3104, F-80039 Amiens Cedex 1, France

Abstract

Among the series of polyanionic positive electrodes for Na-ion batteries having the general formula $\text{Na}_3\text{V}_2(\text{PO}_4)_2\text{F}_{3-y}\text{O}_y$ ($0 \leq y \leq 2$), the composition $\text{Na}_3\text{V}_2(\text{PO}_4)_2\text{F}_3$ ($y = 0$) has the highest theoretical energy that offers competitive electrochemical performances compared to sodium transition metal oxides. Recently the structural phase diagram from $\text{Na}_3\text{V}_2(\text{PO}_4)_2\text{F}_3$ to $\text{Na}_1\text{V}_2(\text{PO}_4)_2\text{F}_3$ has been thoroughly investigated by *operando* synchrotron X-ray diffraction revealing an unexpected structural feature for the end member composition. In fact the crystal structure of $\text{Na}_1\text{V}_2(\text{PO}_4)_2\text{F}_3$ has two very different vanadium environments within each bi-octahedron that suggests a charge disproportionation of two V^{IV} into V^{III} and V^{V} . This work shows an *operando* X-ray absorption spectroscopy at vanadium K-edge during the electrochemical extraction of Na^+ in order to monitor the redox processes involved in this compound. The large data set provided by this experiment has been processed by the principal component analysis combined with multivariate curve resolution. The results suggest that the bi-octahedra have to be considered as the basic structural unit. The peculiar geometry of this material combined with the mixed vanadium valence, directly investigated here along the reaction, seems to allow original electronic configurations. In particular the two vanadium sites into the basic bi-octahedra unit evolves from $\text{V}^{\text{III}} - \text{V}^{\text{III}}$ to $\text{V}^{\text{III}} - \text{V}^{\text{IV}}$ and to a final $\text{V}^{\text{III}} - \text{V}^{\text{IV}}$ configuration. These observations are completed with ^{51}V NMR sensitive to diamagnetic V^{V} .

Introduction

The increasing need for electrochemical energy storage, either for portable electronic devices or for larger-scale applications such as hybrid electric vehicles or static renewable energy storage systems, causes renewed interest in alternatives to Li-ion batteries in order to overcome drawbacks associated to the availability and prize of lithium resources.¹ In this context Na-ion batteries is an emerging field owing to lower price and very large earth-abundance of sodium.² In terms of energy density Na-ion

batteries hardly competes with Li-ion ones due to the intrinsic properties of Na: a less negative standard reduction potential (-2.7 V vs SHE for the $\text{Na}^+_{\text{aq}}/\text{Na}$ against -3.04 V for the $\text{Li}^+_{\text{aq}}/\text{Li}$ one) and a higher molecular weight. Thus Na-ion technology can be addressed for targeted applications such as domestic energy storage and load leveling applications.

Among several polyanionic-based electrode materials,³⁻⁹ one of the most promising family turns out to be the sodium-vanadium fluorophosphate compounds $\text{Na}_3\text{V}_2(\text{PO}_4)_2\text{F}_{3-y}\text{O}_y$ where y can vary from 0 to 2.¹⁰⁻²⁰ This whole range of compositions from V^{III} -rich ($y = 0$) to V^{IV} -rich ($y = 2$), can be oxidized to V^{IV} -rich and V^{V} -rich compounds respectively by the deintercalation of two sodium ions. For instance in $\text{Na}_3\text{V}_2(\text{PO}_4)_2\text{F}_3$ ($y = 0$) the extraction of 2 Na^+ ions has been experimentally demonstrated with two main voltage-composition plateaus at around 3.7 and 4.2 V vs Na^+/Na giving a theoretical energy density of 507 Wh/kg^{17, 21-22} (128 Ah/kg at an average potential of 3.95 V), competitive with that delivered by LiFePO_4 in Li-ion batteries. As recently depicted by Bianchini *et al.*¹⁵ the pristine $\text{Na}_3\text{V}^{\text{III}}_2(\text{PO}_4)_2\text{F}_3$ crystallizes in the *Amam* space group at room temperature. This structure consists of a tridimensional framework of $\text{V}_2\text{O}_8\text{F}_3$ bi-octahedra which are connected by PO_4 tetrahedra that generates large tunnels where Na^+ ions are mobile upon extraction/insertion reactions.

The *operando* structural evolution has been extensively characterized by Bianchini *et al.*¹⁴ who described the phase diagram of $\text{Na}_3\text{V}^{\text{III}}_2(\text{PO}_4)_2\text{F}_3 - \text{Na}_1\text{V}^{\text{IV}}_2(\text{PO}_4)_2\text{F}_3$ as a complex succession of biphasic reactions and solid solution domains. One important and also unexpected feature raised by this study was the assumed charge disproportionation of 2 V^{IV} into 1 V^{V} and 1 V^{III} observed at the end of the charge (*i.e.* after the extraction of 2 Na^+ ions) for the composition $\text{Na}_1\text{V}^{\text{IV}}_2(\text{PO}_4)_2\text{F}_3$ ($\text{Na}_1\text{V}^{\text{IV}}_2\text{PF}$ in the following). Such a charge disproportionation was for instance also observed in $\text{Li}_x\text{V}_2\text{O}_5$,²³ whereas more generally charge separation is commonly observed in inorganic vanadium-rich compounds.²⁴⁻²⁸ Indeed the environment stabilized for vanadium, especially in oxides, changes drastically from an octahedron to a square pyramid with the oxidation state.

The fully charged composition $\text{Na}_1\text{V}_2(\text{PO}_4)_2\text{F}_3$ is described using the *Cmc2₁* space group which has two distinct vanadium crystallographic sites associated to V^{III} and V^{V} instead of only one for the pristine material associated to V^{III} . This hypothesis of charge disproportionation is based on bond valence sum calculations which reveal significant different values for V(1) and V(2): +3.3 and +4.7 respectively. A description of all these features is summarized in **Figure 1**, with a comparison between $\text{Na}_3\text{V}^{\text{III}}_2(\text{PO}_4)_2\text{F}_3$ and $\text{Na}_1\text{V}^{\text{IV}}_2(\text{PO}_4)_2\text{F}_3$ that emphasizes especially the vanadium environments of these two compositions.

In order to directly investigate this proposed disproportionation reaction and thus getting a better insight on the redox processes involved during the sodium extraction from $\text{Na}_3\text{V}_2(\text{PO}_4)_2\text{F}_3$ an *operando* vanadium K-edge X-ray absorption spectroscopy (XAS) study has been performed during the cycling of a $\text{Na}/\text{Na}_3\text{V}_2(\text{PO}_4)_2\text{F}_3$ battery. The collected XAS data are directly sensitive to the

vanadium oxidation state and to the local structure around the vanadium centers. The whole dataset has been analyzed using chemometrics through principal component analysis (PCA) and multivariate curve resolution (MCR). Due to the peculiar environment of the vanadium in this material and its complex behavior during oxidation, the use of linear combinations of well-chosen XAS spectra, either standards or identified compositions upon sodium extraction, turned out to be not possible. The combined use of PCA and MCR offers a blind-source separation method to process a large data set of this *operando* XAS experiment by expressing the data based on their similarities and differences. These methods mainly used for following *in situ* catalysis reaction.²⁹⁻³² Note that this method has also been used to analyze lithium insertion in graphite and lithium extraction in LiFePO_4 via neutron powder diffraction³³ which constitutes a relevant approach to investigate the *operando* behavior of batteries upon cycling. ^{51}V MAS NMR (magic-angle spinning nuclear magnetic resonance) was performed on materials obtained at the end of the charge, close to the composition $\text{Na}_1\text{V}^{\text{IV}}_2(\text{PO}_4)_2\text{F}_3$, in order to confirm the formation of the diamagnetic ion V^{V} (t_{2g}^0) which is in that case the probed nucleus. By the reported results of the combined use of XAS and NMR we were then able to follow the evolution of the local electronic and structural properties as a function of Na content in *operando* conditions and to reveal the coexistence of V^{III} and V^{V} at the end of the charge.

1. Experimental part

The $\text{Na}_3\text{V}_2(\text{PO}_4)_2\text{F}_3$ powder sample was synthesized according to the method already described in details elsewhere.¹⁵ From the direct comparison (given in supplementary information, **Figure S1**) with a previous XAS study performed on $\text{Na}_3\text{V}_2(\text{PO}_4)_2\text{F}_{3-y}\text{O}_y$ ($0 \leq y \leq 0.5$)¹⁹ the amount of V^{IV} defect (y) was estimated to be 0.03 in the as-prepared material. Considering the small content of defects it was neglected in the discussion of the overall mechanism.

Electrodes were prepared by mixing $\text{Na}_3\text{V}_2(\text{PO}_4)_2\text{F}_3$ with Carbon Super P (Csp) as conductive additive and polytetrafluoroethylene (PTFE) as the binder (60:30:10 wt%). The mixture was ground in a mortar until a homogeneous film was obtained. Small pellets of 8 mm diameter and ~ 300 μm thickness were used in an *in situ* cell already described in details elsewhere.³⁴ The electrochemically active part of the cell is obtained from the stacking of the positive electrode, glass fiber separators (Whatman) wetted with a 1 M solution of NaPF_6 (Strem Chemical; 99%) in a mixture of ethylene carbonate and dimethyl carbonate (EC:DMC = 1:1) and sodium metal as the counter electrode. This stacking is inserted between two beryllium windows acting as X-ray-transparent current collectors. The internal pressure within the cell is applied through a spring to ensure an optimal electrical contact. The comparison of

the electrochemistry obtained in this *in-situ* cell is compared in **Figure S2** (given in supplementary information) to that obtained in classical coin cells, excellent reproducibility was obtained.

Vanadium K-edge XAS measurements were collected in the fluorescence mode at the CLÆSS beamline³⁵ of the ALBA Synchrotron (Barcelona, Spain) using a single channel silicon drift detector. The synchrotron radiation of a wiggler source was monochromatized by means of a Si(111) double crystal monochromator. Rh-coated collimating and toroidal mirrors were used to optimize the energy resolution and to reject higher harmonics and to control the beam size at the sample position (0.7 x 1.5 mm²). The calibration of the monochromator was performed by measuring the spectrum of a vanadium metal foil in transmission mode. The absolute energy reproducibility of the measured spectra was ± 0.1 eV. The incoming energy resolution around the vanadium K-edge can be estimated below 0.4 eV. The incoming and, in the case of calibration, outgoing flux have been measured by customized ionization chambers. During the electrochemical cycle, 200 individual spectra were recorded in continuous mode (around 4 min per spectrum) in the XANES (X-ray Absorption Near-Edge Structure) region of vanadium K-edge (5465 eV) with equidistant energy steps of $\Delta E = 0.2$ eV.

First of all, the *operando* XANES spectra were normalized to the atomic absorption estimated by a linear fit to the data in the EXAFS (Extended X-ray Absorption Fine Structure) region after a pre-edge linear background subtraction. To increase the signal-to-noise ratio the scans were merged in bunches of 5 which give a total of 40 spectra representing the complete charge. Then the data were globally analysed using a statistical tool named PCA using the computer program Matlab.³⁶ PCA is a chemometric factor analysis tool generally used to discover the minimal particular structures in multivariate spectral data sets. Here it allows to determine the number of independent component contributing to the whole series of collected spectra during the electrochemical cycling. The number of principal components determined was then used as the basis for Multivariate Curve Resolution-Alternating Least Squares (MCR-ALS) analysis.³⁷⁻³⁸ This algorithm allows the stepwise reconstruction of the spectral components which is necessary for interpreting the whole set of *operando* spectra.

The same electrochemical setup, using classical cells and without binder, was used to prepare the deintercalated compositions near $\text{Na}_1\text{V}^{\text{IV}}_2(\text{PO}_4)_2\text{F}_3$. The cells were charged in galvanostatic mode at a C/20 rate up to 4.3 V vs Na^+/Na , and maintained at this voltage for several hours (C rate is corresponding to the exchange of one electron per hour per mole of compound). The materials as obtained were subsequently washed in DMC to remove any traces of the electrolyte salt and then dried in vacuum. The so-obtained powders were stored under inert atmosphere and subsequently characterized by capillary synchrotron XRD and ⁵¹V MAS NMR. The *ex situ* characterization of the phase pure $\text{Na}_1\text{V}_2(\text{PO}_4)_2\text{F}_3$ is difficult due to its lack of stability because of its high equilibrium potential. It is revealed by the presence, as a secondary phase, of the more reduced composition

$\text{Na}_{1.3}\text{V}_2(\text{PO}_4)_2\text{F}_3$ already identified in a previous work.¹⁴ Its presence as a secondary phase is not an issue since it does not prevent the detection of the possible V^{V} signature in the major phase Na_1VPF .

High resolution Synchrotron powder X-ray diffraction (SXRD) data were collected using the MSPD diffractometer at ALBA (Barcelona, Spain). The powders were placed in a 0.5 mm diameter capillary and data recorded in Debye-Scherrer geometry with a wavelength of 0.9540 Å in the 2θ angular range of $1 - 70^\circ$ with a 0.005° step and an accumulation time of 6 minutes.

^{51}V MAS NMR spectra were recorded on a Bruker Avance III 500 MHz spectrometer (131.5 MHz resonance frequency for ^{51}V) using a standard Bruker 2.5 mm MAS probe with a 30 kHz typical spinning frequency. The recycle time $D_0 = 0.2$ s is long enough to avoid T_1 saturation effects. The baseline distortions resulting from the spectrometer dead time (5-10 μs) were removed computationally using a polynomial baseline correction routine. $\alpha\text{-VOPO}_4$ with a single V site that exhibits a signal located at -765 ppm³⁹ was used as secondary reference.

2. Results and discussion

Figure 2 displays the electrochemical data obtained during the *operando* XAS experiment at the rate of C/10 up to 4.4 V vs. Na^+/Na as a function of the number of normalized collected spectra. The so-obtained electrochemical curve is identical to those already reported in previous studies.¹⁴⁻¹⁵ **Figure 2** displays also a series of selected XAS spectra obtained during the charge between $\text{Na}_3\text{V}^{\text{III}}_2(\text{PO}_4)_2\text{F}_3$ (Na_3VPF - purple line) and $\text{Na}_1\text{V}^{\text{IV}}_2(\text{PO}_4)_2\text{F}_3$ (Na_1VPF - brown line). The inset focuses on the pre-edge region.

Vanadium K-edge XANES exhibits several features as already largely testified by experimental and theoretical studies.⁴⁰⁻⁴² The main absorption edge, at around 5485 eV, is related to the valence state of the transition metal and corresponds to the strong contribution of the $1s \rightarrow 4p$ dipole allowed transition. The weak pre-edge contributions around 5470 eV, arise from $1s \rightarrow 3d$ forbidden quadrupolar transitions that become allowed by orbital $3d$ - p hybridizations.⁴⁰ Both energy positions and intensity distributions of the pre-peak signals are linked to the electronic structure and the local structural environment of the probed element.

Firstly, the overall 2.5 eV shift of the main absorption edge towards higher energy from $\text{Na}_3\text{V}^{\text{III}}_2(\text{PO}_4)_2\text{F}_3$ (around 5484.5 eV) to $\text{Na}_1\text{V}^{\text{IV}}_2(\text{PO}_4)_2\text{F}_3$ (around 5487 eV) is consistent with an increase of the vanadium average oxidation state. Pre-edge lines are complex to identify and attribute precisely since there are several contributions all along the electrochemical oxidation of NVPF. It can be stated however that their evolution is consistent with the increase of vanadium oxidation state since the contributions at higher energy are growing and the overall integrated intensity is increasing. In

fact, an increase of the contribution at higher energy can be ascribed to a progressive modification/distortion of the local symmetry⁴⁰ that leads to an increasing $3d-4p$ orbital mixing, that means a larger overlap of the $3d$ vanadium orbitals with the $2p$ oxygen orbitals. This mixing enhances the theoretically forbidden $1s \rightarrow 3d$ transition, inducing an increase in the pre-edge intensity.⁴³

During sodium deintercalation, the vanadium oxidation state is expected to increase linearly, and the absorption edge is supposed to evolve in the same way. However the energy position of the main absorption edge shows a nonlinear evolution, in a way strongly correlated to the electrochemical data. In fact, a rapid evolution is observed between spectra 17 and 20, together with the sudden increase of potential in the voltage curve (**Figure 3**). This particular evolution suggests that the whole set of data cannot be described as a simple linear combination of the initial and final spectra, as it could have been expected for a process characterized by the gradual vanadium oxidation from the average V^{III} to V^{IV} oxidation state. In fact more complex processes seem to occur during the redox reaction suggesting unexpected local electronic rearrangements. From this finding and the impossibility to do relevant comparisons with known references due to the specific environment of vanadium in the $Na_3V_2(PO_4)_2F_3$ framework (*i.e.* in $V_2O_8F_3$ bi-octahedra displayed in **Figure 1**) data were analyzed using principal component analysis (PCA) combined with multivariate curve resolution (MCR). In order to avoid an over-interpretation of the experimental data and to extract the maximum amount of useful information from the *operando* XANES spectra PCA was performed on the whole dataset. In this method each spectrum is considered as an n -dimensions vector (n corresponding to the number of measured absorption points). All measured spectra form a matrix, which can be reduced to its lowest dimensionality by the use of orthogonal factor space: this factor analysis is the principal component analysis (*i.e.* PCA).

The first principal component has the largest initial variance, *i.e.*, alone it takes into account as much as possible the whole set of data. The following principal components are built orthogonal to the first one, and allow the reproduction of the experimental spectra with the highest possible variance *via* adapted linear combinations of them. An orthogonal basis of uncorrelated components whose the dimension is less than or equal to the number of original spectra is thus obtained. In the different linear combinations which are built to reconstruct each experimental spectrum, the multiplication factors of the principal components are commonly called scores.

The variance plot obtained from PCA analysis given in **Figure 4** shows rather clearly that about 99.9 % of the variance of the XANES spectra can be described using only three principal components, the residual part being supposedly due to experimental noise. A visualisation of the evolution of the respective scores comforts this hypothesis, with both shape and contribution of the first three components varying gradually through the different processes (as expected in a gradual evolution of

the studied material during oxidation) and those of the following ones changing in a totally erratic way, thus probably representing mainly experimental noise.

Even though the so-obtained principal components are only orthogonal mathematical functions and not real XANES spectra, their determination reveals the number of independent spectral components that can be used to fit the whole set of experimental data. Several methodologies are then available to reconstruct the corresponding real XANES components as well as their evolution such as the MCR-ALS (Multivariate Curve Resolution - Alternating Least Squares) analysis tool.³⁷⁻³⁸ A detailed description of this method from a theoretical point of view is given by Tauler et al.⁴⁴⁻⁴⁵ who was the first to propose this method for the analysis of *in situ* spectroscopic data. On the other hand, the intrinsic limits of the application of this method are discussed in ref.⁴⁶ In this work, the MCR-ALS analysis was performed by applying the following constraints for both spectral components and their respective concentrations, in order to reproduce a physically and chemically meaningful behavior: (i) non-negativity of the concentrations of the components, (ii) unimodality for one of the three components (only a single highest value of concentration) and (iii) closure (sum of the 3 components always equal to 100% of the intensity). MCR-ALS method converged after 25 iterations with a variance of 99.998 %.

As a result, the three XANES spectra shown in **Figure 5** were obtained together with the evolution of their concentration along the electrochemical reaction path. According to the evolution of their relative concentrations, the three XANES spectra can be described as follows: the first component (C1) corresponds to the pristine electrode material $\text{Na}_3\text{V}^{\text{III}}_2(\text{PO}_4)_2\text{F}_3$ and the third component (C3) to the desodiated material $\text{Na}_1\text{V}^{\text{IV}}_2(\text{PO}_4)_2\text{F}_3$ obtained at the charged state. However the second component (C2) seems to be an intermediate component since it cannot be identified as a given composition. Concerning the evolution of their relative intensities, on the first voltage plateau it appears that C1 is continuously decreasing while C2 is increasing. On the other hand once the voltage jump is reached C3 starts growing while both C1 and C2 decrease gradually.

The XANES spectra extracted from the MCR-ALS analysis are in good agreement with the observations made considering the quantitative evolutions of the components: C1 and C3 are, as expected, almost identical to the first (number 1) and the last (number 40) *operando* measured XANES spectra, respectively. Since C2 never reaches 100 % of the relative quantity it cannot be identified with a measured spectrum. Comparing the absorption energy of the main edge jump obtained for each component, 5484.5 eV for C1, 5485.8 eV for C2 and 5486.9 eV for C3, it appears that it evolves linearly as a function of the oxidation state of vanadium, as expected, if the component C2 represents a composition with an average oxidation state between V^{III} and V^{IV} , very close to $\text{V}^{+3.5}$. Besides, during the first voltage plateau only V^{III} and V^{IV} are expected to be present, so C2 can reasonably be ascribed to a mixture of about 50 % of V^{III} and 50 % of V^{IV} . Assuming these

hypotheses, *i.e.* an average oxidation state of +3 for C1, +3.5 for C2 and +4 for C3, the overall average oxidation state which can be calculated from the relative quantities evolution is compared in **Figure 6** to the actual oxidation state expected from the electrochemical experiment. It shows a rather good agreement despite a small deviation from the theoretical oxidation state given by the straight blue line.

It is worth noticing that the evolution of the three components is much more simple compared to the complex phase diagram previously reported by Bianchini *et al.*¹⁴ that revealed complex structures showing for some of them commensurate modulations and thus complex charge and/or ionic rearrangements upon sodium extraction. Considering the peculiar framework whose basic units are the $V_2O_8F_3$ bi-octahedra linked to each other by phosphates (see **Figure 1**), and that each vanadium has another vanadium in its local environment (V-V interatomic distance within $V_2O_8F_3$ bi-octahedron: 3.96 Å), and only one (as the next V-V distance is: 4.73 Å), it is reasonable to assume that the components obtained here which are associated to local environments seen by XAS reflect the local pair arrangement. The three components can thus be expressed by the local pair arrangements $V^{III}-V^{III}$ for C1, $V^{III}-V^{IV}$ for C2 and $V^{IV}-V^{IV}$ for C3 (or $V^{III}-V^V$ in case of charge disproportionation) within vanadium bi-octahedron.

The pre-edge show four main contributions observed at 5466, 5468, 5469.5 and 5471 eV with different relative intensities along sodium deintercalation. As no fully relevant standards were found, it was difficult to give a full interpretation for each of the contribution. Nevertheless the increase from C1 to C3 of the whole pre-edge integrated intensity and the shift towards higher energies of the average energy position are in agreement with the decrease of the number of *d* electrons in the vanadium electronic configuration and to the increasing distortion of the octahedral coordination of the vanadium centres, thus with an increasing probability of the *1s* to *3d* transitions.

In **Figure 7** we report the measured absorption pre-peak, the corresponding MCR calculated one and their corresponding difference. Considering the residues of the difference between the measured and the calculated data, they are subtle but still observable within the pre-edge. They could be attributed to slight modifications of the components along the reaction that are too small to be taken into account by the PCA as well by the MCR analysis. This could be responsible for the small deviation from the actual oxidation state mentioned before and shown in **Figure 6**, this limited “discrepancy” highlighting the accuracy of this mathematical analysis.

Nevertheless at this point of the study there is no clear proof of the presence of V^V in the material. Comparing the spectrum obtained previously by Serras *et al.*⁴⁷ at the end of the charge for the compound $Na_1V_2(PO_4)_2F_{1.4}O_{1.6}$ (showing an average oxidation state of +4.5 and thus a non-negligible amount of V^V) gives only indirect but already interesting information. In this case the presence of the V^V is mainly associated to the growth of a peak around 5471 eV in the pre-edge region. In our case, as depicted in **Figures 2 and 5** a similar phenomenon is observed as a peak at 5471 eV rises concomitant

with the appearance of C3 which might indicate that the charge disproportionation is occurring at the first voltage jump from the extraction of the second Na^+ ion. It is interesting to notice, that there is a delay in the apparition of the peak at 5471 eV in the spectra calculated using the MCR components compared to the experimental ones. This observation could explain the slightly lower average oxidation state of vanadium found by MCR compared to the one expected from electrochemistry.

In order to ensure the presence of V^{V} ions in the fully oxidized compound ^{51}V MAS NMR was used. Indeed, NMR signals have been observed by high resolution MAS NMR at room temperature only for compounds contained diamagnetic V^{V} ions as observed for $\alpha\text{-VOPO}_4$ that was used as secondary reference.⁴⁸ Firstly, in order to assess the quality of the compound measured by ^{51}V MAS NMR, a SXRD pattern was preliminary collected in a sealed capillary to prevent contact with ambient air.

SXRD data of the near fully charged material were analyzed by Rietveld refinement using $Cmc2_1$ and $I4/mmm$ space groups to describe Na_1VPF and $\text{Na}_{1.3}\text{VPF}$ respectively as displayed in **Figure 8**. This material is composed of 63 % of $\text{Na}_1\text{V}^{\text{IV}}(\text{PO}_4)_2\text{F}_3$ and 27 % of $\text{Na}_{1.3}\text{V}_2(\text{PO}_4)_2\text{F}_3$ and its corresponding ^{51}V NMR MAS spectra are compared to those of $\text{Na}_3\text{V}_2(\text{PO}_4)_2\text{F}_3$, and $\alpha\text{-VOPO}_4$. In agreement with literature $\alpha\text{-VOPO}_4$ exhibits a single narrow signal (-765 ppm) and a set of spinning side bands.³⁹ The absence of significant quadrupolar second-order lineshape indicates that the quadrupolar interaction is moderate.

No signals were observed for ^{51}V in $\text{Na}_3\text{V}^{\text{III}}_2(\text{PO}_4)_2\text{F}_3$, as expected. The NMR spectrum shows however, some residual spinning sidebands of ^{23}Na MAS NMR signal, as the sodium (^{23}Na) and vanadium (^{51}V) resonance frequencies are very close 132.3 and 131.5 MHz respectively. For the charged compound composed of 63 % of $\text{Na}_1\text{V}_2(\text{PO}_4)_2\text{F}_3$ and 27 % of $\text{Na}_{1.3}\text{V}_2(\text{PO}_4)_2\text{F}_3$, the spectrum exhibits clearly signals located in the [-650, -850] ppm region and their corresponding spinning sidebands. These signals are assigned to V^{5+} ions present in the charged compound. The signal located around -680 ppm may be assigned to V^{5+} in $\text{Na}_1\text{V}_2(\text{PO}_4)_2\text{F}_3$ which is the major phase present and the others to V^{5+} ions in $\text{Na}_{1.3}\text{V}_2(\text{PO}_4)_2\text{F}_3$ that may exhibit different environments versus Na^+ .

The presence of V^{V} in the near charged state of the battery indicates that V^{V} has to be considered in the redox processes. As previously proposed by Bianchini *et al.*,¹⁴ charge disproportionation really occurs and this information is contained in the third component that can be ascribed to $\text{Na}_1\text{V}^{\text{III}}\text{V}^{\text{V}}(\text{PO}_4)_2\text{F}_3$. The C3 quantity starts growing concomitantly with the voltage jump indicating that a partial charge disproportionation occurs from the average composition $\text{Na}_2\text{V}^{\text{III}}\text{V}^{\text{IV}}(\text{PO}_4)_2\text{F}_3$.

In summary a possible explanation can be given if $\text{V}_2\text{O}_8\text{F}_3$ bi-octahedra within this peculiar framework is considered to be one entity. During the first voltage plateau it is easier to oxidize $\text{V}^{\text{III}}\text{-V}^{\text{III}}$ rather than a $\text{V}^{\text{III}}\text{-V}^{\text{IV}}$ entity whence the formation of $\text{V}^{\text{III}}\text{-V}^{\text{IV}}$ pairs up to reach $\text{Na}_2\text{V}^{\text{III}}\text{V}^{\text{IV}}(\text{PO}_4)_2\text{F}_3$ (*i.e.* average oxidation state +3.5). Once the $\text{Na}_2\text{V}^{\text{III}}\text{V}^{\text{IV}}(\text{PO}_4)_2\text{F}_3$ configuration is reached further sodium extraction (*i.e.* oxidation) leads to the formation of $\text{V}^{\text{III}}\text{-V}^{\text{V}}$ pairs. The appearance of the charge disproportionation

at this point of the charge is likely due to the fact that the structure does not allow the formation of V^{IV} - V^{IV} pair in $V_2(PO_4)_2F_3$ bi-octahedra.

Conclusion

Based on structural observations it has been proposed by Bianchini *et al.* that a charge disproportionation of $2V^{IV}$ into V^{III} and V^V occurs in $Na_1V^{IV}_2(PO_4)_2F_3$.¹⁴ In this study ^{51}V MAS NMR has confirmed the presence of the diamagnetic ions V^V in the near fully deintercalated materials supporting that the charge disproportionation actually occurs. Furthermore, *operando* vanadium K-edge XANES study has shown that this phenomena does not occur only at the end of the charge, but immediately after the extraction of one Na^+ ion *i.e.* after reaching the composition $Na_2V^{III}V^{IV}(PO_4)_2F_3$. One way to understand this feature is to consider the bi-octahedra, and not the octahedra, as the basic structural unit. This peculiar geometry combined with mixed valence seems to allow electronic exchanges that induce original configurations. The characterization of these electronic exchanges is crucial in order to establish the groundwork required to fully understand the sodium extraction/insertion mechanism combined with electronic properties in this compound and might be extended to other related compounds having this bi-octahedron geometry with the composition $V_2(PO_4)_2F_{3-x}O_x$.

Supporting Information

Comparison of XAS spectra for $Na_3V_2(PO_4)_2F_{3-y}O_y$ ($0 \leq y \leq 0.5$) and electrochemical results obtained in in-situ cells and in classical coin cells

Acknowledgments

The authors thank Matteo Bianchini (ILL/LRCS/ICMCB) for his technical assistance and fruitful discussions, also C. Marini and W. Olszewski at CLÆSS beamline at ALBA (Barcelona, Spain) for their help while preparing the XAS experiment and MSPD beamline at ALBA for Synchrotron X-ray diffraction, and G. Gachot (LRCS) for fruitful discussions on the electrolyte. The authors also acknowledge RS2E for the funding of TB's postdoctoral fellowship. This project has received funding from Région Nouvelle Aquitaine, the French National Research Agency (STORE-EX Labex Project ANR-10-LABX-76-01 and SODIUM Descartes project ANR-13-RESC-0001-02), and the European Union's Horizon 2020 research and innovation program under grant agreement No 646433-NAIADES.

References

1. Tarascon, J.-M., Is lithium the new gold? *Nature chemistry* **2010**, *2*, 510.
2. Palomares, V.; Serras, P.; Villaluenga, I.; Hueso, K. B.; Carretero-González, J.; Rojo, T., Na-ion batteries, recent advances and present challenges to become low cost energy storage systems. *Energy & Environ. Sci.* **2012**, *5*, 5884-5901.
3. Jian, Z.; Han, W.; Lu, X.; Yang, H.; Hu, Y. S.; Zhou, J.; Zhou, Z.; Li, J.; Chen, W.; Chen, D., Superior electrochemical performance and storage mechanism of $\text{Na}_3\text{V}_2(\text{PO}_4)_3$ cathode for room-temperature sodium-ion batteries. *Adv. Energy Mater.* **2013**, *3*, 156-160.
4. Sauvage, F.; Quarez, E.; Tarascon, J.-M.; Baudrin, E., Crystal structure and electrochemical properties vs. Na^+ of the sodium fluorophosphate $\text{Na}_{1.5}\text{VOPO}_4\text{F}_{0.5}$. *Solid State Sci.* **2006**, *8*, 1215-1221.
5. Shakoor, R.; Seo, D.-H.; Kim, H.; Park, Y.-U.; Kim, J.; Kim, S.-W.; Gwon, H.; Lee, S.; Kang, K., A combined first principles and experimental study on $\text{Na}_3\text{V}_2(\text{PO}_4)_2\text{F}_3$ for rechargeable Na batteries. *J. Mater. Chem.* **2012**, *22*, 20535-20541.
6. Liu, Z.-M.; Wang, X.-Y.; Ying, W.; Tang, A.-P.; Yang, S.-Y.; He, L.-F., Preparation of $\text{NaV}_{1-x}\text{Al}_x\text{PO}_4\text{F}$ cathode materials for application of sodium-ion battery. *Trans. Nonferrous Met. Soc. China* **2008**, *18*, 346-350.
7. Chihara, K.; Kitajou, A.; Gocheva, I. D.; Okada, S.; Yamaki, J.-I., Cathode properties of $\text{Na}_3\text{M}_2(\text{PO}_4)_2\text{F}_3$ [M= Ti, Fe, V] for sodium-ion batteries. *J. Power Sources* **2013**, *227*, 80-85.
8. Kim, H.; Shakoor, R.; Park, C.; Lim, S. Y.; Kim, J. S.; Jo, Y. N.; Cho, W.; Miyasaka, K.; Kahraman, R.; Jung, Y., $\text{Na}_2\text{FeP}_2\text{O}_7$ as a promising iron-based pyrophosphate cathode for sodium rechargeable batteries: a combined experimental and theoretical study. *Adv. Funct. Mater.* **2013**, *23*, 1147-1155.
9. Masquelier, C.; Croguennec, L., Polyanionic (phosphates, silicates, sulfates) frameworks as electrode materials for rechargeable Li (or Na) batteries. *Chem. Rev.* **2013**, *113*, 6552-6591.
10. Serras, P.; Palomares, V.; Goñi, A.; de Muro, I. G.; Kubiak, P.; Lezama, L.; Rojo, T., High voltage cathode materials for Na-ion batteries of general formula $\text{Na}_3\text{V}_2\text{O}_{2x}(\text{PO}_4)_2\text{F}_{3-2x}$. *J. Mater. Chem.* **2012**, *22*, 22301-22308.
11. Serras, P.; Palomares, V.; Goñi, A.; Kubiak, P.; Rojo, T., Electrochemical performance of mixed valence $\text{Na}_3\text{V}_2\text{O}_{2x}(\text{PO}_4)_2\text{F}_{3-2x}/\text{C}$ as cathode for sodium-ion batteries. *J. Power Sources* **2013**, *241*, 56-60.
12. Park, Y.-U.; Seo, D.-H.; Kwon, H.-S.; Kim, B.; Kim, J.; Kim, H.; Kim, I.; Yoo, H.-I.; Kang, K., A new high-energy cathode for a Na-ion battery with ultrahigh stability. *J. Am. Chem. Soc.* **2013**, *135*, 13870-13878.
13. Park, Y. U.; Seo, D. H.; Kim, H.; Kim, J.; Lee, S.; Kim, B.; Kang, K., A Family of high-performance cathode materials for Na-ion batteries, $\text{Na}_3(\text{VO}_{1-x}\text{PO}_4)_2\text{F}_{1+2x}$ ($0 \leq x \leq 1$): combined first-principles and experimental study. *Adv. Funct. Mater.* **2014**, *24*, 4603-4614.
14. Bianchini, M.; Fauth, F.; Brisset, N.; Weill, F.; Suard, E.; Masquelier, C.; Croguennec, L., Comprehensive investigation of the $\text{Na}_3\text{V}_2(\text{PO}_4)_2\text{F}_3$ - $\text{NaV}_2(\text{PO}_4)_2\text{F}_3$ system by operando high resolution synchrotron X-ray diffraction. *Chem. Mater.* **2015**, *27*, 3009-3020.
15. Bianchini, M.; Brisset, N.; Fauth, F.; Weill, F.; Elkaim, E.; Suard, E.; Masquelier, C.; Croguennec, L., $\text{Na}_3\text{V}_2(\text{PO}_4)_2\text{F}_3$ revisited: a high-resolution diffraction study. *Chem. Mater.* **2014**, *26*, 4238-4247.
16. Tsirlin, A.; Nath, R.; Abakumov, A.; Furukawa, Y.; Johnston, D.; Hemmida, M.; von Nidda, H.-A. K.; Loidl, A.; Geibel, C.; Rosner, H., Phase separation and frustrated square lattice magnetism of $\text{Na}_{1.5}\text{VOPO}_4\text{F}_{0.5}$. *Phys. Rev. B* **2011**, *84*, 014429.
17. Gover, R.; Bryan, A.; Burns, P.; Barker, J., The electrochemical insertion properties of sodium vanadium fluorophosphate, $\text{Na}_3\text{V}_2(\text{PO}_4)_2\text{F}_3$. *Solid State Ionics* **2006**, *177*, 1495-1500.
18. Song, W.; Ji, X.; Wu, Z.; Zhu, Y.; Li, F.; Yao, Y.; Banks, C. E., Multifunctional dual $\text{Na}_3\text{V}_2(\text{PO}_4)_2\text{F}_3$ cathode for both lithium-ion and sodium-ion batteries. *RSC Adv.* **2014**, *4*, 11375-11383.
19. Broux, T.; Bamine, T.; Fauth, F.; Simonelli, L.; Olszewski, W.; Marini, C.; Ménétrier, M.; Carlier, D.; Masquelier, C.; Croguennec, L., Strong impact of the oxygen content in $\text{Na}_3\text{V}_2(\text{PO}_4)_2\text{F}_{3-y}\text{O}_y$ ($0 \leq y \leq 0.5$) on its structural and electrochemical properties. *Chem. Mater.* **2016**, *28*, 7683-7692.

20. Ponrouch, A.; Dedryvère, R.; Monti, D.; Demet, A. E.; Mba, J. M. A.; Croguennec, L.; Masquelier, C.; Johansson, P.; Palacín, M. R., Towards high energy density sodium ion batteries through electrolyte optimization. *Energy Environ. Sci.* **2013**, *6*, 2361-2369.
21. Barker, J.; Gover, R.; Burns, P.; Bryan, A., Hybrid-ion a lithium-ion cell based on a sodium insertion material. *Electrochem. Solid-State Lett.* **2006**, *9*, A190-A192.
22. Barker, J.; Gover, R.; Burns, P.; Bryan, A., $\text{Li}_{4/3}\text{Ti}_{5/3}\text{O}_4 \parallel \text{Na}_3\text{V}_2(\text{PO}_4)_2\text{F}_3$: An example of a hybrid-ion cell Using a Non-graphitic Anode. *J. Electrochem. Soc.* **2007**, *154*, A882-A887.
23. Rao, K.; Pecquenard, B.; Gies, A.; Levasseur, A.; Etourneau, J., Structural and electrochemical behaviour of sputtered vanadium oxide films: oxygen non-stoichiometry and lithium ion sequestration. *Bull. Mater. Sci.* **2006**, *29*, 535-546.
24. Schindler, M.; Hawthorne, F.; Baur, W., Crystal chemical aspects of vanadium: polyhedral geometries, characteristic bond valences, and polymerization of (VO_n) polyhedra. *Chem. Mater.* **2000**, *12*, 1248-1259.
25. Seo, H.; Fukuyama, H., Charge ordering and spin gap in NaV_2O_5 . *J. Phys. Chem. Solids* **1999**, *60*, 1095-1097.
26. Nakao, H.; Ohwada, K.; Takesue, N.; Fujii, Y.; Isobe, M.; Ueda, Y.; Zimmermann, M. v.; Hill, J.; Gibbs, D.; Woicik, J., X-Ray Anomalous Scattering Study of a charge-ordered state in NaV_2O_5 . *Phys. Rev. Lett.* **2000**, *85*, 4349.
27. Ballhausen, C. J.; Gray, H. B., The electronic structure of the vanadyl ion. *Inorg. Chem.* **1962**, *1*, 111-122.
28. Ohama, T.; Yasuoka, H.; Isobe, M.; Ueda, Y., Mixed valency and charge ordering in NaV_2O_5 . *Phys. Rev. B* **1999**, *59*, 3299-3302.
29. Voronov, A.; Urakawa, A.; van Beek, W.; Tsakoumis, N. E.; Emerich, H.; Rønning, M., Multivariate curve resolution applied to in situ X-ray absorption spectroscopy data: An efficient tool for data processing and analysis. *Anal. Chim. Acta* **2014**, *840*, 20-27.
30. Rochet, A.; Baubet, B.; Moizan, V.; Devers, E.; Hugon, A.; Pichon, C.; Payen, E.; Briois, V., Influence of the preparation conditions of oxidic $\text{NiMo}/\text{Al}_2\text{O}_3$ catalysts on the sulfidation ability: a quick-XAS and raman spectroscopic study. *J. Phys. Chem. C* **2015**, *119*, 23928-23942.
31. Cassinelli, W. H.; Martins, L.; Magnani, M.; Pulcinelli, S. H.; Briois, V.; Santilli, C. V., Time-resolved XAS/MS/Raman monitoring of mutual copper self-reduction and ethanol dehydrogenation reactions. *RSC Adv.* **2016**, *6*, 20453-20457.
32. Cassinelli, W. H.; Martins, L.; Passos, A. R.; Pulcinelli, S. H.; Santilli, C. V.; Rochet, A.; Briois, V., Multivariate curve resolution analysis applied to time-resolved synchrotron X-ray Absorption Spectroscopy monitoring of the activation of copper alumina catalyst. *Catal. Today* **2014**, *229*, 114-122.
33. Rodriguez, M. A.; Van Benthem, M. H.; Ingersoll, D.; Vogel, S. C.; Reiche, H. M., In situ analysis of LiFePO_4 batteries: signal extraction by multivariate analysis. *Powder Diffraction* **2010**, *25*, 143-148.
34. Leriche, J.; Hamelet, S.; Shu, J.; Morcrette, M.; Masquelier, C.; Ouvrard, G.; Zerrouki, M.; Soudan, P.; Belin, S.; Elkaïm, E., An electrochemical cell for operando study of lithium batteries using synchrotron radiation. *J. Electrochem. Soc.* **2010**, *157*, A606-A610.
35. Simonelli, L.; Marini, C.; Olszewski, W.; Avila Perez, M.; Ramanan, N.; Guilera, G.; Cuartero, V.; Klementiev, K., CLÆSS: The hard x-ray absorption beamline of the ALBA CELLS synchrotron. *Cogent Phys.* **2016**, *3*, 1231987.
36. Massart, D. L.; Vandeginste, B. G. M.; Buydens, L. M. C.; Jong, S. D.; Lewi, P. J.; Smeyers-Verbeke, J., Handbook of Chemometrics and Qualimetrics: Part A. **1997**, 1-867.
37. Jaumot, J.; de Juan, A.; Tauler, R., MCR-ALS GUI 2.0: New features and applications. *Chemometr. Intell. Lab.* **2015**, *140*, 1-12.
38. Jaumot, J.; Gargallo, R.; de Juan, A.; Tauler, R., A graphical user-friendly interface for MCR-ALS: a new tool for multivariate curve resolution in MATLAB. *Chemometr. Intell. Lab.* **2005**, *76*, 101-110.
39. Siegel, R.; Dupré, N.; Querton, M.; Hirschinger, J., ^{51}V magic angle spinning NMR in VOPO_4 phases. *Magn. Reson. Chem.* **2004**, *42*, 1022-1026.
40. Wong, J.; Lytle, F.; Messmer, R.; Maylotte, D., K-edge absorption spectra of selected vanadium compounds. *Phys. Rev. B* **1984**, *30*, 5596.

41. Poumellec, B.; Kraizman, V.; Aifa, Y.; Cortes, R.; Novakovich, A.; Vedrinskii, R., Experimental and theoretical studies of dipole and quadrupole contributions to the vanadium K-edge XANES for VOPO₄·2H₂O xerogel. *Phys. Rev. B* **1998**, *58*, 6133.
42. Wu, Z.; Xian, D.; Hu, T.; Xie, Y.; Tao, Y.; Natoli, C.; Paris, E.; Marcelli, A., Quadrupolar transitions and medium-range-order effects in metal K-edge x-ray absorption spectra of 3d transition-metal compounds. *Phys. Rev. B* **2004**, *70*, 033104.
43. Salem, S.; Chang, C.-N.; Nash, T., Energy shift and structure of the K-absorption edge of vanadium in some vanadium compounds. *Phys. Rev. B* **1978**, *18*, 5168.
44. Tauler, R., Multivariate curve resolution applied to second order data. *Chemometr. Intell. Lab. Syst.* **1995**, *30*, 133-146.
45. De Juan, A.; Tauler, R., Chemometrics applied to unravel multicomponent processes and mixtures: revisiting latest trends in multivariate resolution. *Anal. Chim. Acta* **2003**, *500*, 195-210.
46. Ruckebusch, C.; Blanchet, L., Multivariate curve resolution: a review of advanced and tailored applications and challenges. *Anal. Chim. Acta* **2013**, *765*, 28-36.
47. Serras, P.; Palomares, V.; Alonso, J.; Sharma, N.; López del Amo, J. M.; Kubiak, P.; Fdez-Gubieda, M. L.; Rojo, T. f., Electrochemical Na extraction/insertion of Na₃V₂O_{2x}(PO₄)₂F_{3-2x}. *Chem. Mater.* **2013**, *25*, 4917-4925.
48. Jordan, B.; Calvo, C., Crystal structure of α-VPO₅. *Can. J. Chem.* **1973**, *51*, 2621-2625.

Figure captions

Figure 1: Cristal structures of $\text{Na}_3\text{V}_2(\text{PO}_4)_2\text{F}_3$ and $\text{Na}_1\text{V}_2(\text{PO}_4)_2\text{F}_3$ with PO_4 in green, VO_4F_2 octahedra in blue and Na atoms in red. In $\text{Na}_1\text{V}_2(\text{PO}_4)_2\text{F}_3$ significant different vanadium environments are highlighted with light and dark blue corresponding to regular and distorted environments respectively.

Figure 2: Top: voltage as a function of the spectrum number and corresponding to the galvanostatic charge obtained at C/10 during *operando* XAS data collection. Bottom: *operando* vanadium K-edge XANES spectra collected during the charge. The inset is focused on the pre-edge region.

Figure 3: Left: voltage (black line) as a function of the spectrum number and corresponding to the galvanostatic charge obtained at C/10 during *operando* XAS data collection with the associated 1st derivative (blue line). Right: 2D projection of *operando* vanadium K-edge XANES spectra collected during the charge and emphasizing discontinuities at voltage jumps.

Figure 4: Variance plot of PCA analysis. Evolution of the scores of the 6 first components.

Figure 5: Top: three components extracted from MCR analysis. The inset is focused on the pre-edge region. Bottom: evolution of the relative quantities of the three principal components compared with the experimental electrochemical data (black solid line).

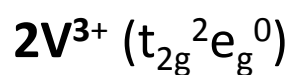
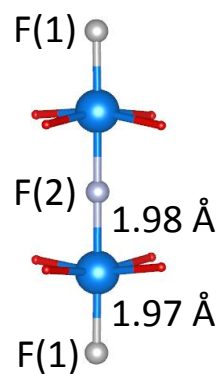
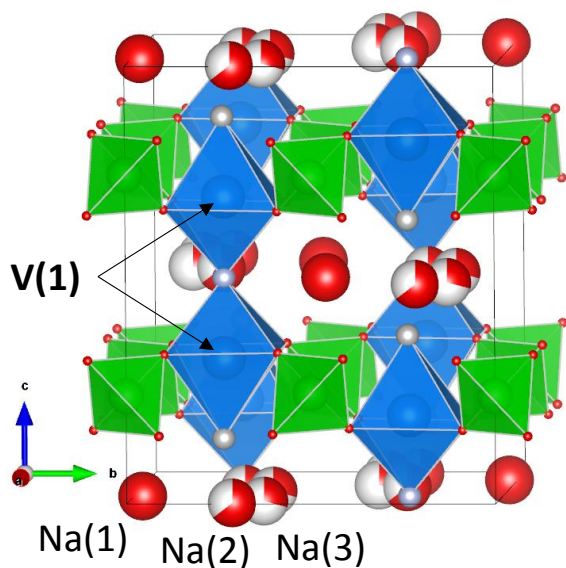
Figure 6: Experimental electrochemical curve (black solid line) associated to the expected oxidation state (blue solid line). The blue dotted line represents the oxidation state calculated from the relative quantities of the three components associated with their observed oxidation state: C1 = +3; C2 = +3.5 and C3 = +4.

Figure 7: 2D projection of *operando* vanadium K-edge XANES spectra of the pre-edge – Top: measured data – Middle: reconstructed data from MCR analysis – Bottom: difference between the measured data and the reconstructed data.

Figure 8: Top: Rietveld refinement of the electrochemically oxidized compound using $\text{Cmc}2_1$ and $\text{I}4/\text{mmm}$ space groups for Na_1VPF and $\text{Na}_{1.35}\text{VPF}$ respectively. Bottom: ^{51}V MAS NMR spectra NMR of the electrochemically oxidized compound (red line), of the pristine material Na_3VPF (purple line) and of $\text{V}^{\text{V}}\text{PO}_4\text{O}$ (green line).

Figure 1

$\text{Na}_3\text{V}_2(\text{PO}_4)_2\text{F}_3$ - Space group: *Amam*



$\text{Na}_1\text{V}_2(\text{PO}_4)_2\text{F}_3$ - Space group: *Cmc2_1*

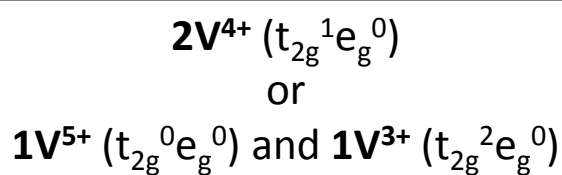
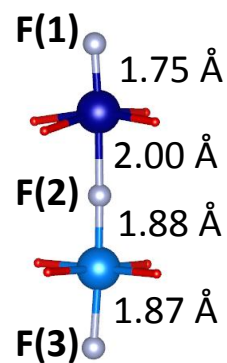
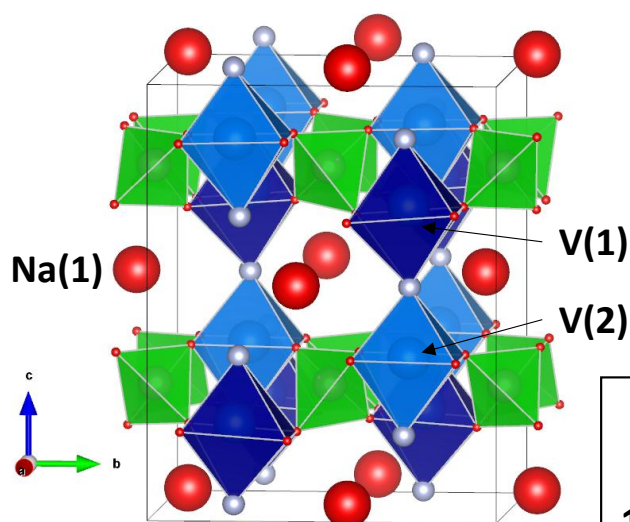


Figure 2

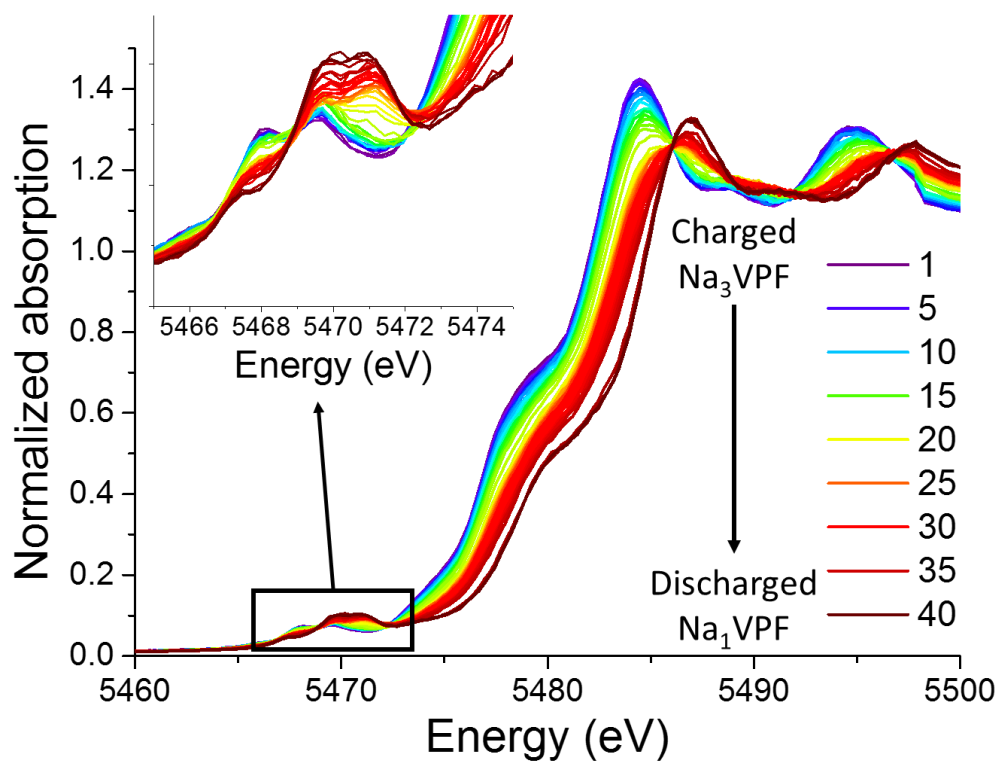
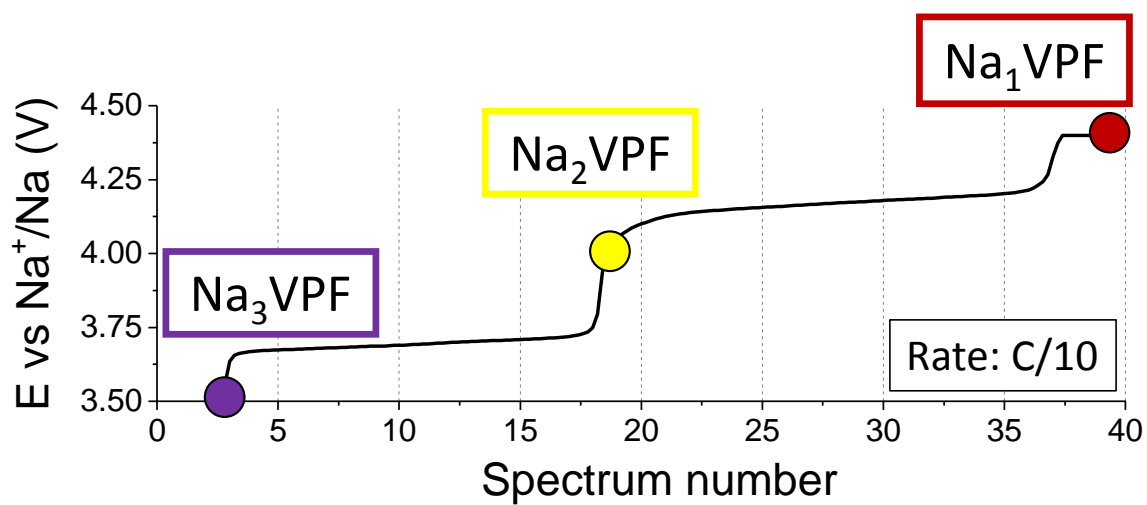


Figure 3

Please this figure has to be a two columns figure

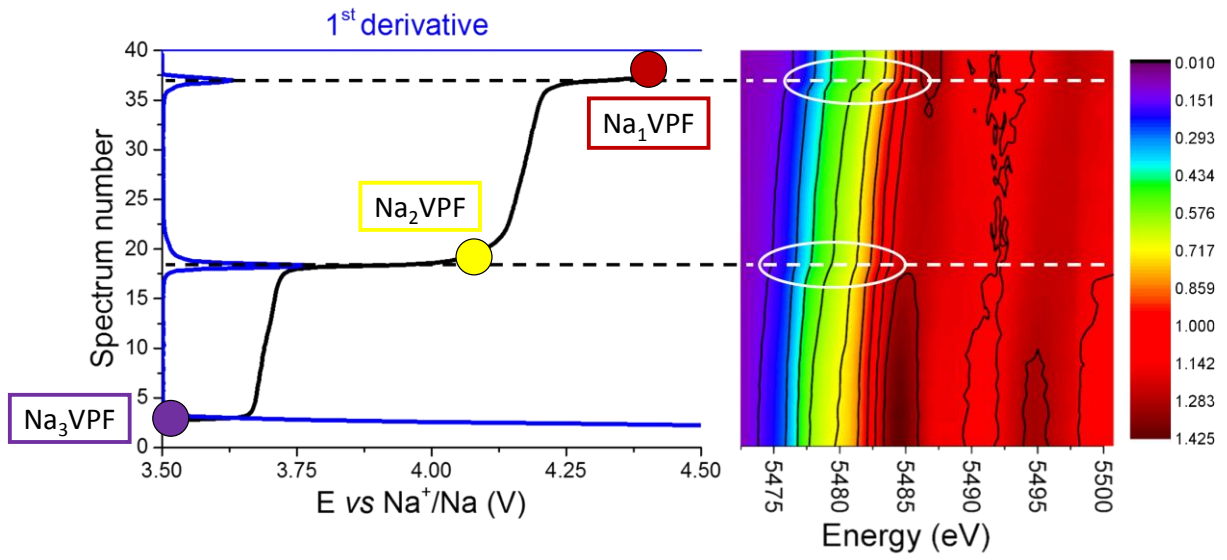


Figure 4

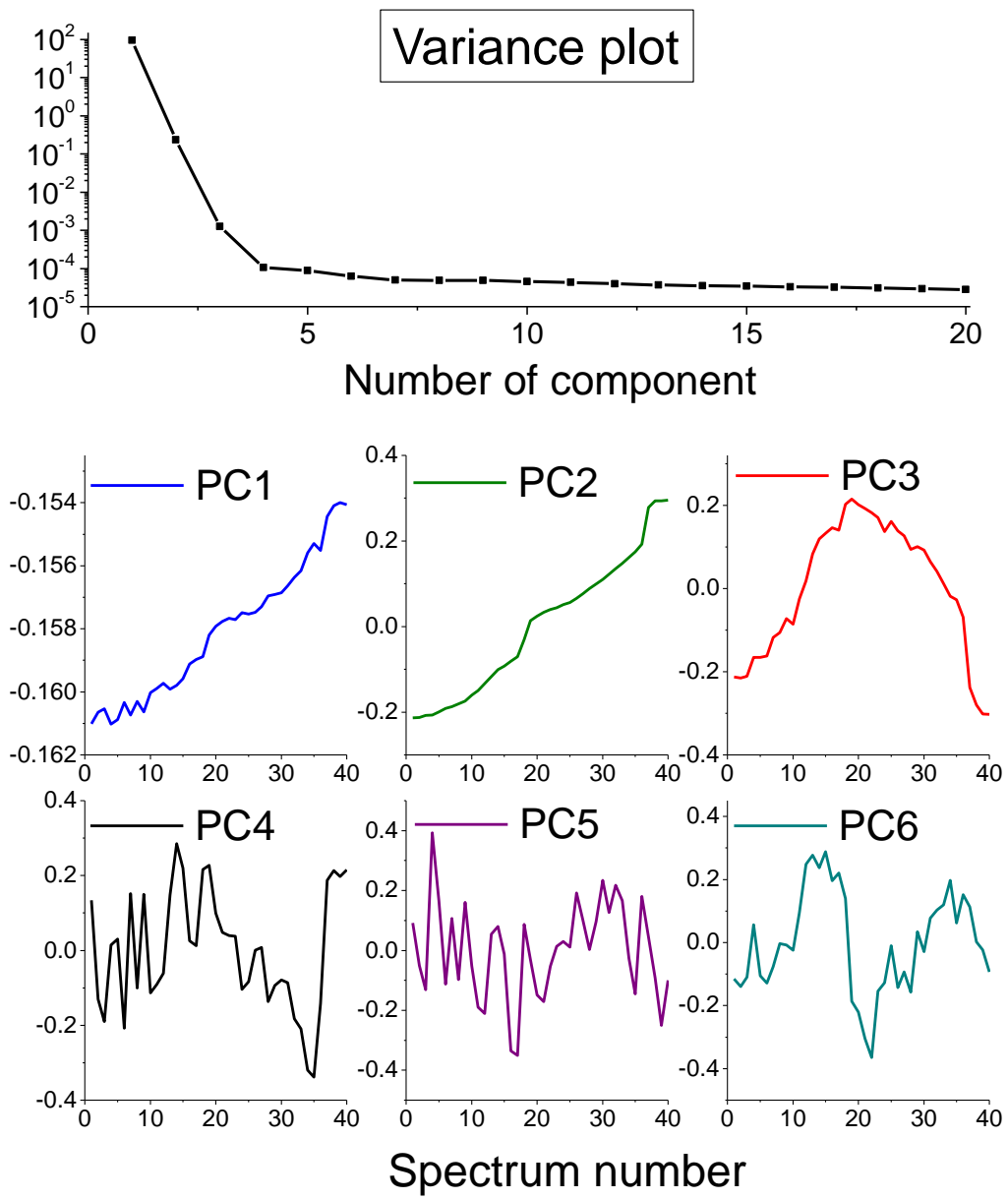


Figure 5

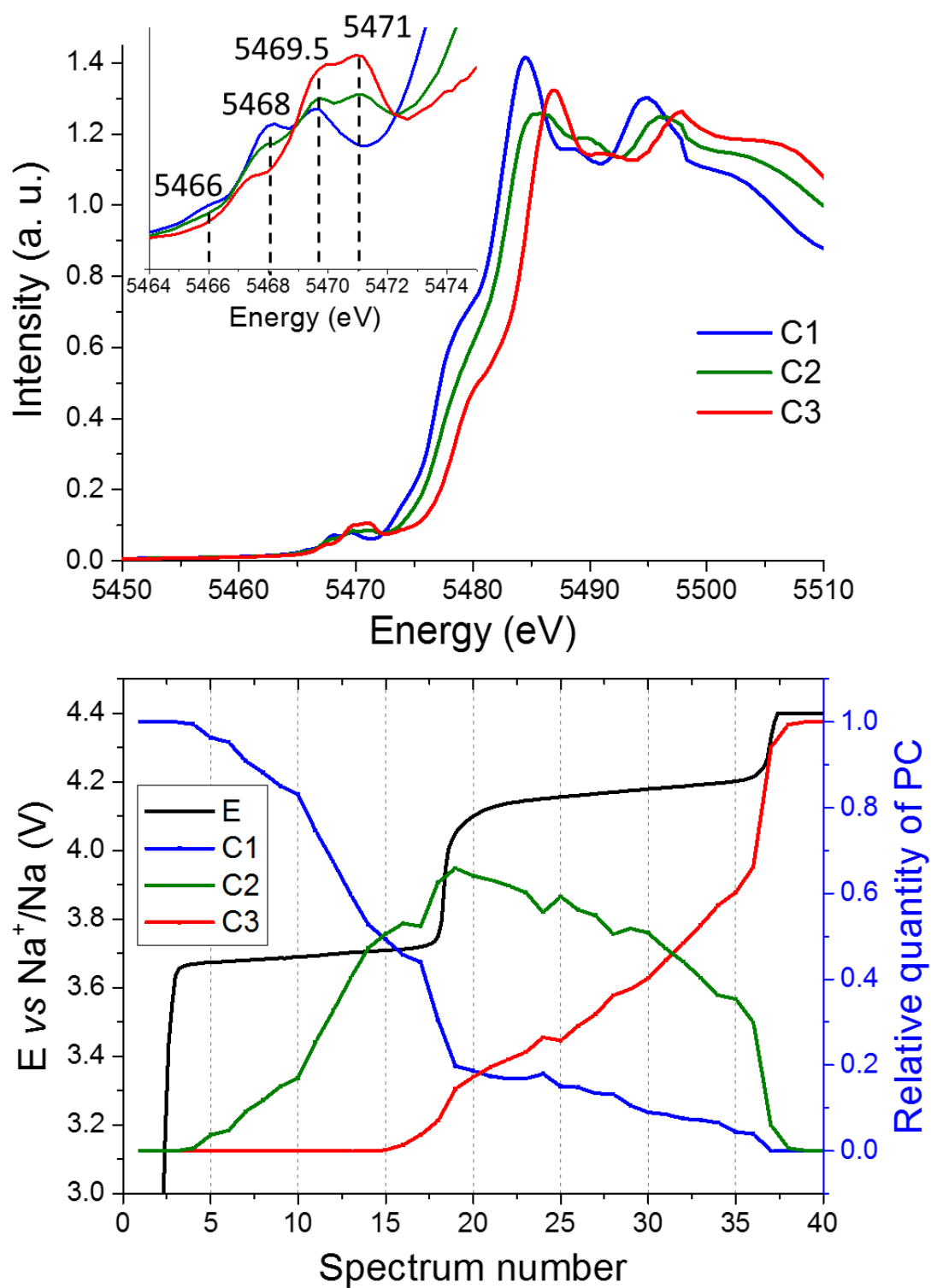


Figure 6

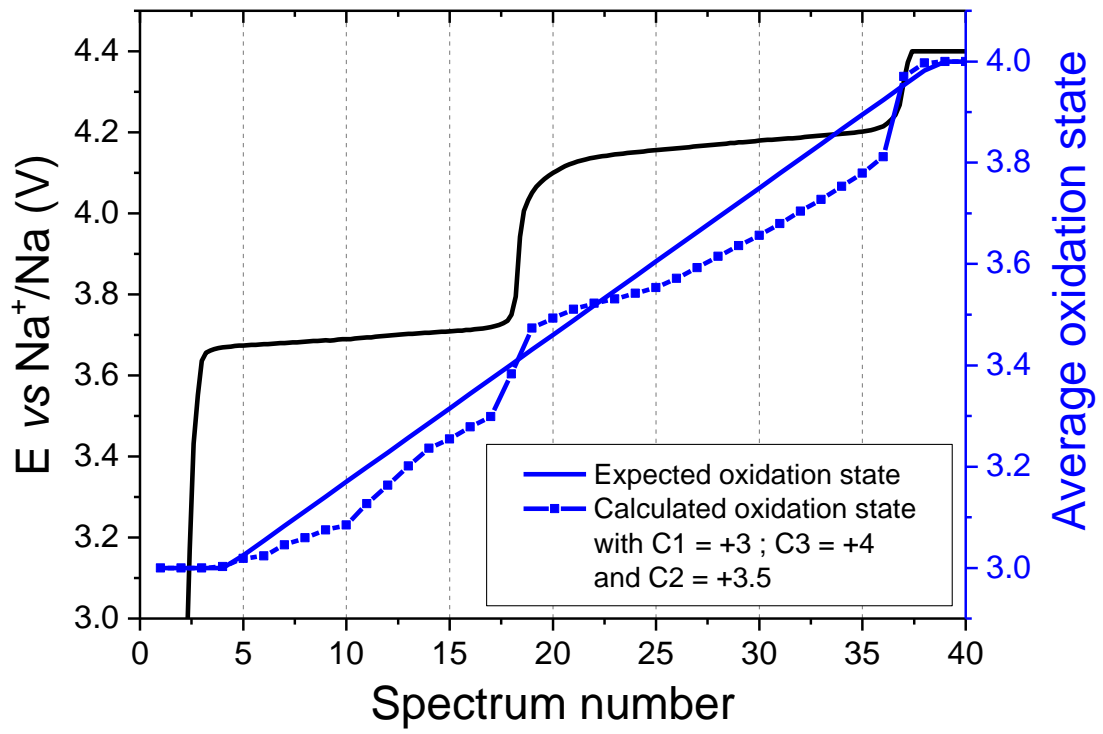


Figure 7

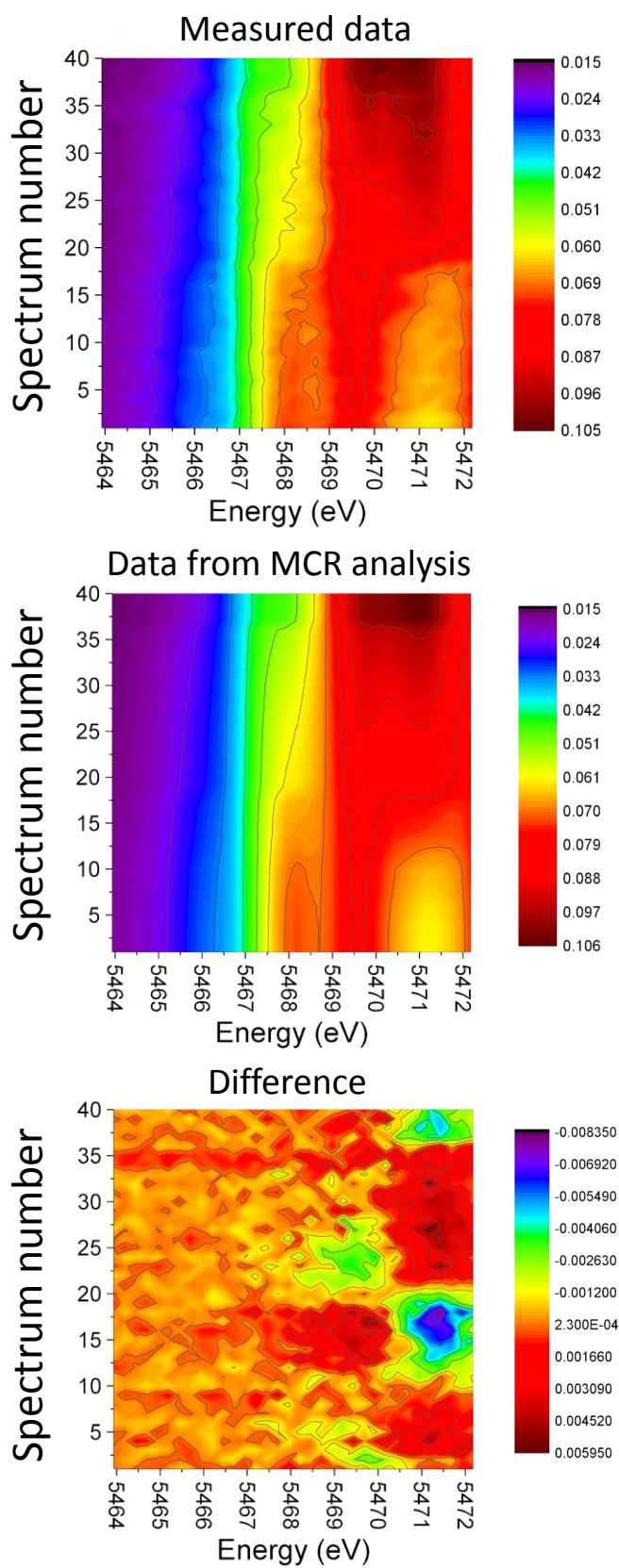


Figure 8

